

A Fluka Study of Underground Cosmogenic Neutron Production

A. Empl,¹ E. V. Hungerford, R. Jasim and P. Mosteiro^b

Department of Physics, University of Houston, Houston, TX 77204

^bDepartment of Physics, Princeton University, Princeton, NJ 08544

E-mail: aempl@central.uh.edu

Abstract. Neutrons produced by cosmic muon interactions are important contributors to backgrounds in underground detectors when searching for rare events. Typically such neutrons can dominate the background, as they are particularly difficult to shield and detect. Since actual data is sparse and not well documented, simulation studies must be used to design shields and predict background rates. Thus validation of any simulation code is necessary to assure reliable results. This work compares in detail predictions of the FLUKA simulation code to existing data, and uses this code to report a simulation of cosmogenic backgrounds for typical detectors embedded in a water tank with liquid scintillator shielding.

Keywords: Muon, Cosmic, Cosmogenic, Neutron, Borexino, DarkSide

¹Corresponding author.

Contents

1	Introduction	1
2	FLUKA	2
2.1	The FLUKA Code	2
2.2	Physics models in FLUKA	2
2.3	Physics related user options	3
3	Cosmogenic background simulation at LNGS	4
3.1	Muon radiation field	4
3.1.1	Intensity	4
3.1.2	Mean energy and differential energy spectrum	4
3.1.3	Angular distribution	5
3.1.4	Bundles	6
3.1.5	Event generation	6
3.2	Muon-induced secondaries	7
3.2.1	Geometry	7
3.2.2	Propagation through rock	7
3.2.3	Particle components of the muon-induced radiation field	8
3.3	Connection of simulation to measured muon event flux	8
4	Validation	8
4.1	The Borexino experiment	8
4.2	Benchmark results	9
4.2.1	Muon-induced neutron yield	9
4.2.2	^{11}C isotope production	11
4.2.3	Cosmogenic isotope production	12
4.2.4	Distance between neutron capture location and muon track	12
4.2.5	Neutron multiplicity	14
4.2.6	Muon rate producing neutrons	14
5	Cosmogenic background predictions for DarkSide	15
5.1	Detector geometry	15
5.1.1	Counting Test Facility	16
5.1.2	Liquid-Scintillator neutron Veto	17
5.1.3	Inner detector	17
5.2	Simulation results	17
6	Conclusions	20

1 Introduction

This paper reports the use of the FLUKA simulation code to study muon-induced, cosmogenic backgrounds. It is particularly interested in predicted neutron backgrounds for direct neutrino and dark matter experiments, and additionally in the production of radio-isotopes in the detector

shielding. Typically, such experiments are placed in deep underground facilities where only neutrinos and high energy muons are able to reach the detectors. In this study, special care was taken to validate FLUKA with available data, and by comparing our results with previous simulations. Muons induce backgrounds by producing showers of secondary particles in local interactions in, or near, the detector. As only high energy muons penetrate to the depth of the experimental halls, the total muon flux decreases as the lower energy, more intense muons, are removed from the spectrum. Consequently, the mean energy of the residual muons increases with depth.

Little experimental information about muon-induced secondaries at depth is available. Most previous studies concentrated on the neutron flux in the muon radiation field. Low rates and challenges inherent in neutron measurements require careful interpretation of the available data. Indeed, measurements of neutron production at deep underground sites was previously suggested as a method to study the incident muon flux at such facilities [1]. As a consequence, neutron yield was measured at increasing depth for many years [2]-[7]. However, such information was limited to cosmogenic neutrons, mostly in large, liquid-scintillator detectors, where the flux was determined by measuring the emitted gamma radiation after neutron capture in the scintillator. Thus detector geometry and efficiency affected the interpretation of the data, and experiments had to rely on the simulation of particle interactions and transport to extract and predict the muon-induced backgrounds. Interpretation of the early measurements was (and is) challenging, since systematic uncertainties are large and usually underestimated.

2 FLUKA

2.1 The FLUKA Code

FLUKA [8, 9] is a fully integrated particle-physics, Monte Carlo simulation package, originally introduced to aid in shielding design of particle accelerators. More recently it has been applied in high energy particle physics, medical physics, radio-biology, and of relevance here, to simulate cosmic ray and cosmogenic backgrounds in deep underground experiments.

Design and development of FLUKA has always been based on the implementation of verified microscopic models of physical processes. FLUKA uses these models in a way which maintains consistency among all the reaction steps and types. Thus, all conservation laws are enforced at each step and predictions are benchmarked against experimental data, if possible, at the level of single interactions. This results in a consistent approach to all energy/target/projectile combinations with a minimal overall set of free parameters. As a consequence, predictions for complex simulation problems are robust and arise naturally from underlying physical models. Depending on model validity, FLUKA is expected to provide reasonable results even in cases where no direct experimental data are available [10].

The version of FLUKA used for the present study is FLUKA2011.2, from November 2011. A collection of benchmark results for the physical aspects of the code relevant to the problem of muon-induced backgrounds are presented in [11].

2.2 Physics models in FLUKA

Production of cosmogenic neutrons in FLUKA is the result of direct muon nuclear interactions, photo-nuclear reactions by real photons in electromagnetic showers, and in nuclear cascades within resulting hadronic showers. Direct muon-nuclear interactions are modeled by μ^- capture at rest, and by virtual photo-nuclear interactions. The latter are factorized following Bezrukov-Bugaev [12] into virtual photon production and photon-nucleus reactions. The photon-nucleus reactions are simulated over the entire energy range through different mechanisms:

- Giant Resonances interaction,
- Quasi-Deuteron effect,
- Delta Resonances production, and
- Vector Meson Dominance at high energies.

Hadronic interactions in FLUKA are described in several papers ([13]-[16]). Hadron-nucleon inelastic collisions up to a few GeV are realized in terms of resonance production and decay. At higher energies, the simulation employs a modified Dual Parton Model [16]. The Dual Parton Model is a quark/parton string model providing reliable results up to several tens of TeV.

The FLUKA nuclear interaction model called PEANUT [36] can be schematically described as a sequence of the following steps:

- Glauber-Gribov cascade in high energy collisions,
- Generalized-Intra-Nuclear cascade,
- Pre-equilibrium emission, and
- Evaporation/Fragmentation/Fission and de-excitation.

Some of these steps may be skipped depending on the projectile energy and type. PEANUT is a precise and reliable tool for intermediate energy hadron-nucleus reactions. Its “nuclear environment” is also used in the simulation of real and virtual photo-nuclear reactions, neutrino interactions, nucleon decays and muon captures. All nuclear interaction models, including nucleus-nucleus interactions, share parts of the common PEANUT framework. In particular, all nuclear fragments, irrespective of how they are produced, are de-excited through a common evaporation/fragmentation and gamma production chain. A validation of the FLUKA Monte Carlo code for predicting induced radioactivity is given in [17].

2.3 Physics related user options

The physics models in FLUKA are fully integrated into the code, and the individual models are benchmarked against available experimental data. The user is presented with an overall optimized configuration of models which cannot be user adjusted.

The simulation reported here was performed with the FLUKA default setting PRECISIO(n). In addition, photo-nuclear interactions were enabled through the FLUKA option PHOTONUC and the detailed treatment of nuclear de-excitation was requested with the EVAPORAT(ion) and COALESCE(nce) options. The latter two options are suggested to the user in order to obtain more reliable results for isotope production. These enable the evaporation of heavy fragments ($A > 1$) and the emission of energetic light-fragments, respectively. The treatment of nucleus-nucleus interactions was also turned on for all energies via the option IONTRANS, and delayed reactions were enabled through the option, RADDECAY.

Neutron captures on hydrogen inside liquid scintillator are recorded in order to evaluate the muon-induced neutron production rate. This approach closely follows that of any such experimental measurement and avoids technical ambiguities for neutron counting.

3 Cosmogenic background simulation at LNGS

A faithful simulation of the muon radiation field in the vicinity of any underground experiment requires detailed information of the depth, overburden geometry, and composition of the rock surrounding the detector through which the muons propagate. Since the cavern size is small relative to changes in the flux, the radiation field can be assumed constant at the average depth of the experimental hall. However, details of the detector geometry and materials surrounding the cavern and detector must be included in any accurate simulation.

This study differs from previous work in that it includes multi-muon events. As will be seen later, this improves the description of the radiation field. A common approach found in previous literature in context of predicting the neutron yield in liquid scintillator makes use of mono-energetic muons with a mean kinetic energy corresponding to the average depth of the underground site. This study finds that the predicted neutron yield decreases by approximately 8% if mono-energetic muons of 280 GeV are replaced by muons of an appropriate differential energy spectrum having the same mean value for the kinetic energy. However, if muon bundles are properly included, an overall increase in neutron yield on the order of 4% results.

3.1 Muon radiation field

3.1.1 Intensity

The muon flux in the 3 halls at the Italian *Laboratori Nazionali del Gran Sasso* (LNGS) for Underground research is summarized in a recent publication [18]. More precisely, the measured flux describes the total cosmogenic muon event rate, since individual events may contain more than one muon [19]. Variations in muon flux between the measurements given in Table 1 may be attributed to the relative location of the halls within the laboratory, differences in time periods of data collection, and perhaps more importantly, the systematic uncertainties. The value of the flux given by Borexino located in Hall C was adopted for the present simulation.

experiment	Hall	year published	total muon event rate ($\times 10^{-4} \text{ s}^{-1} \text{ m}^{-2}$)
LVD	A	2009	3.31 ± 0.03
MACRO	B	2002	3.22 ± 0.08
Borexino	C	2012	3.41 ± 0.01

Table 1. The table shows the measured muon flux in the various experimental halls at the LNGS

3.1.2 Mean energy and differential energy spectrum

The underground muon kinetic energy spectrum can be represented by the following (for example [20]):

$$\frac{dN}{dE_\mu} = \text{const} \cdot (E_\mu + \epsilon(1 - e^{-\beta h}))^{-\alpha}$$

In the above equation, E_μ is the muon kinetic energy at slant depth h , and α is the surface muon spectral index, and the quantities β and ϵ are related to muon energy loss mechanisms in rock. The average muon kinetic energy at slant depth h is:

$$\langle E_\mu \rangle = \frac{\epsilon(1 - e^{-\beta h})}{\alpha - 2}$$

Experimental results for the spectral index α and the mean muon energy for LNGS were reported by MACRO [20] and are reproduced in Table 3.1.2:

event type	mean muon energy (GeV)	spectral index α
single muon	$270 \pm 3 \text{ (stat)} \pm 18 \text{ (syst)}$	$3.79 \pm 0.02 \text{ (stat)} \pm 0.11 \text{ (syst)}$
double muon	$381 \pm 13 \text{ (stat)} \pm 21 \text{ (syst)}$	$3.25 \pm 0.06 \text{ (stat)} \pm 0.07 \text{ (syst)}$

Table 2. The mean energy of single and double muon events as measured by MACRO

The functional description of the energy spectrum given by equation (3.1.2) permits direct sampling since it can be integrated and inverted in analytic form. Adopting the values $\epsilon = 0.392 \times 10^{-3}$ and $\beta = 635$ GeV this procedure reproduces the measured mean energy for single and double muon events respectively, and yields an overall mean residual energy of 283 ± 19 GeV for cosmogenic muons at LNGS.

3.1.3 Angular distribution

The slant depth of the muon transit through the rock overburden depends on both azimuthal and zenith angles. The azimuthal angular dependence of the slant depth in rock, h ($g\text{ cm}^{-2}$) at LNGS, depends on the profile of the Gran Sasso mountain covering the experimental cavern. Hence, both the intensity and energy profiles of the muons are a function of their incident direction on the detector.

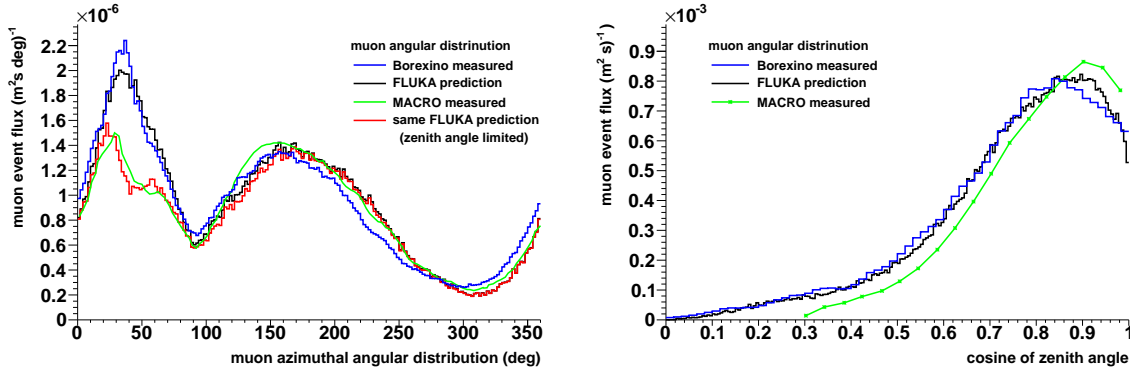


Figure 1. Muon azimuthal (left) and zenith (right) angular distribution at LNGS for polar coordinate system pointing up and North with clockwise increasing angle. Blue line: Borexino data, green line: MACRO data, black (red) line: FLUKA predictions (zenith angle limited).

A measurement of the cosmogenic muon angular distribution at LNGS was performed by MACRO [21] for Hall B. Azimuthal (left) and zenith (right) projections of the distribution are shown by the green histograms in Figure 1. The distributions are compared to recent results from Borexino [22] given by the blue histograms. The difference in the experimental azimuthal spectra for angles near 45 degrees is due to an angular acceptance limit in the zenith angle of approximately 60 degree in MACRO. These data are compared to a FLUKA simulation which traced muons, initiated by cosmic rays in the upper atmosphere, to the experimental halls [23],

and was normalized to the Borexino measured total muon flux. The predictions for full detector acceptance are shown by the black histograms in Figure 1. When the limitation of zenith angle in MACRO is imposed in FLUKA, the same features found in the data are reproduced. The resulting azimuthal spectrum is shown by the red histogram. Good agreement is found between data and simulations, and the small visible shift in the azimuthal distribution is due to the change of location for the two experiments.

3.1.4 Bundles

Muon bundles were investigated at LNGS by the LVD and MACRO experiments. The experimental results used here were taken from MACRO [24]. Figure 2 shows the measured muon multiplicity (left) and the spatial separation between muons for double muon events (right). A simulation to study muon multiplicity used simplified sampling of the distribution up to a muon multiplicity of 4. The distance between muons within a bundle was chosen according to the distribution measured for double muon events, and all muons within a bundle are given the same direction.

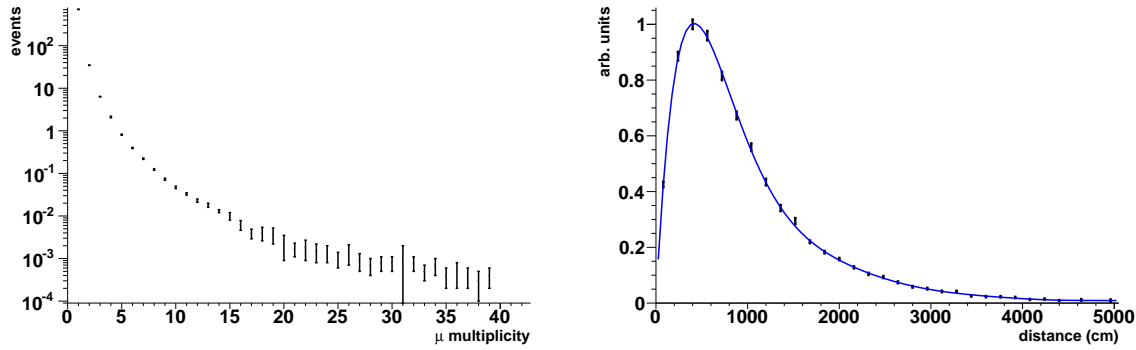


Figure 2. (left) Multiplicity of muons recorded by the MACRO detector for cosmogenic muon events. (right) Spatial separation of muons obtained for cosmogenic events in the MACRO detector featuring two coincident muons (black data points). The blue line shows a simple higher order polynomial fit used to implement sampling of the distribution.

The effect of multi-muon events for the Borexino detector geometry was evaluated assuming the measured multi-muon event rate from MACRO of approximately 6%. Close to 1.5% of the muon events in Borexino feature more than one muon. In addition, about 12% of the single muons crossing the Borexino inner detector belong to multi-muon events.

3.1.5 Event generation

To generate the muon flux within the experimental hall, a combination of azimuthal and zenith angles is selected according to the measured muon angular distribution. A map of the LNGS (Gran Sasso mountain) overburden, which was prepared by the MACRO collaboration [23, 25], is used to translate the muon direction into the respective slant depth h . Next, the muon event type is set to either a single muon or muon bundle. In the case of muon bundles, a multiplicity of up to 4 muons is sampled from the measured multiplicity spectrum. The probability for muon events with larger multiplicity is less than 0.2% and these events are treated as muon bundles of multiplicity 4 to simplify the calculation.

Finally, the muon kinetic energy as a function of slant depth h and muon event type is selected by sampling from the parameterized single or double muon event energy spectra. The

latter is used for muon bundle events of all multiplicities since no experimental information is available for events with higher muon multiplicities.

An important difference between positive and negative muons arises from negative muon capture on nuclei. This effect can produce energetic neutrons, in some cases over 100 MeV. However, at the LNGS depth the fraction of stopping muons is less than 1%. A constant charge ratio of $N_{\mu^+/\mu^-} = 1.38$ was selected to simplify the simulation. This value is consistent with the weighted average of the reported measurements for single and multi-muon events by OPERA [26]: $R_{single} = 1.395 \pm 0.025$ and $R_{multi} = 1.23 \pm 0.1$.

3.2 Muon-induced secondaries

3.2.1 Geometry

The cosmogenic radiation field at deep underground sites is composed of muons and muon-induced secondaries. Incident muons are allowed to develop particle showers as they pass through a 700 cm thick layer of Gran Sasso rock [25] surrounding all sides of Hall C. The amount of rock to fully develop the shower was determined by simulation. Particle production rates for muons of 280 GeV kinetic energy in Gran Sasso rock are reported in Figure 3 (left). Constant particle production rates, indicating full shower development, are reached for a rock thickness of 300-400 cm. However for computational purposes, this thickness was divided into three sections to permit simulation of electromagnetic processes with increasing detail as the shower approached the cavern.

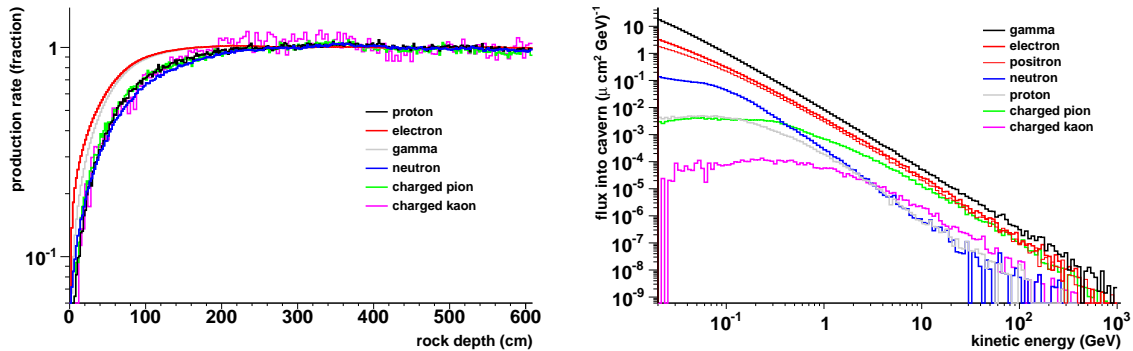


Figure 3. (left) Particle production rates by 280 GeV muons in Gran Sasso rock as function of distance travelled. The rates are normalized per particle species to the maximum production rate. (right) Predicted integral particle flux into Hall C at LNGS per cosmogenic muon event given as a function of particle kinetic energy.

Muon events are randomly placed on a sufficiently large plane located above the hall geometry in order to fully illuminate the hall containing the detector. Other muon tracks outside this envelope are rejected. The basic assumption of this procedure is to implement an initial distribution of muons at every point within the rock with appropriate direction and energy.

3.2.2 Propagation through rock

The cosmogenic radiation which is present at the cavern walls is approximated in two separate steps to reduce computation time. In the first step, the muon radiation field as described in the previous section, is reproduced on a rock layer surrounding Hall C, and allowed to propagate without interactions through the rock. These muons are recorded if they entered the hall. For high

energy, the muon trajectory is approximately unchanged by interactions, so that these recorded muons were chosen as the muon sample for the simulation. They were then propagated a second time with all physics processes enabled in order to obtain a description of the cosmogenic radiation field, including all muon-induced secondaries. The secondaries were recorded along with the muons as part of the incident flux. The sampled muon kinetic energy was adjusted for the average muon energy loss in the rock layer.

3.2.3 Particle components of the muon-induced radiation field

As previously indicated, high energy muons produce many particle types in addition to neutrons. These particles, including the primary muon, can continue to produce backgrounds as they interact with the detector and its surroundings. Figure 3 (right) shows the kinetic energy spectra for the most frequently produced secondaries. Aside from muons, photo-production can also contribute to backgrounds, including neutron backgrounds, due to the large photon flux even though electromagnetic cross sections are small. In order to assess cosmogenic backgrounds, the full muon-induced radiation field needs to be considered rather than, for example, simulating only cosmogenic neutrons. The character of the background problem may be significantly changed considering additional coincident charged secondaries.

3.3 Connection of simulation to measured muon event flux

The muon flux per simulated event, Φ_{sim} as determined above, is then allowed to interact with the detector and shielding. An empty spherical volume was inserted inside the cavern, and exposed to the muon radiation field in order to determine the flux incident on the Borexino detector. The muon fluence estimated by the track length-density inside the sphere was obtained by a standard FLUKA scoring option. Choosing a spherical volume correctly accounts for the angular distribution of the muons. Moreover, the fluence rate through a sphere is a direct estimator of the flux through the cross-sectional area of the sphere.

The length of the time-period considered in the simulation (lifetime), is given by the number of simulated muon events compared to the ratio of the simulated to measured total muon flux, Φ_{exp} , from Table 1.

$$T[s] = N_{events} \cdot \frac{\Phi_{sim}[events^{-1}cm^{-2}]}{\Phi_{exp}[s^{-1}cm^{-2}]}$$

4 Validation

4.1 The Borexino experiment

The most recent, and also the most precise experimental data on cosmogenic neutrons deep underground, are available from the Borexino experiment [22]. The reduced systematic uncertainties of the reported results are primarily a consequence of the very large detector with its un-segmented and shielded spherical liquid scintillator target. In addition, Borexino has a comparatively short recovery time from the large prompt muon signal. This allows less extrapolation and less accidental background between the muon and capture signals. The experimental results and a comparison with Monte Carlo predictions are presented in [22]. These simulations were based on FLUKA using the muon radiation field at LNGS as developed in the previous section.

A cross-sectional view of the FLUKA geometry implemented for the Borexino experiment is given in Figure 4. The central sensitive liquid scintillator region of radius 425 cm has a mass of

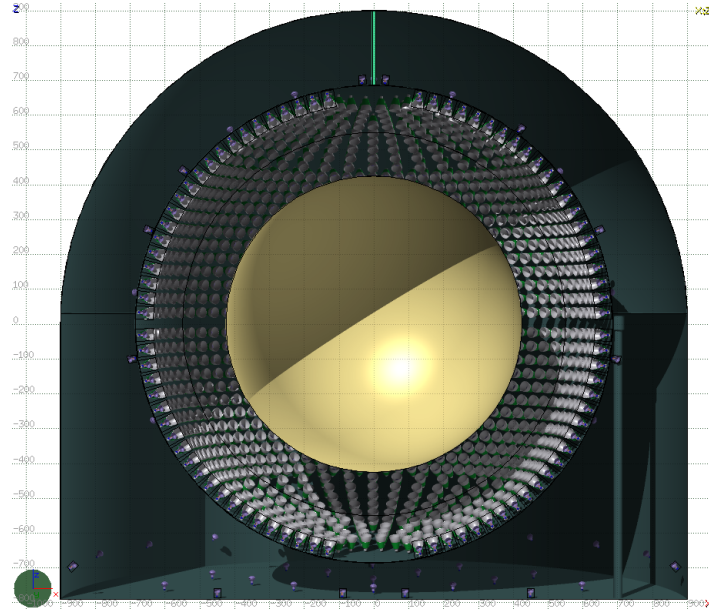


Figure 4. A view of the Borexino detector geometry implemented in FLUKA. The sensitive volume of the Borexino detector, the Inner Vessel, is shown by the golden sphere. It is centered inside two (transparent) buffer regions which are contained inside a stainless steel sphere which supports the optical modules. This inner detector is placed inside a domed, cylindrical water tank which functions as a Čerenkov detector to identify and help track cosmogenic muons.

approximately 278 tons and is contained in a spherical, nylon inner vessel. The detector is located at the center of a 685 cm radius stainless steel sphere filled with quenched liquid scintillator as a passive shield. The stainless steel sphere in turn is placed inside a 900 cm radius cylindrical water tank providing additional shielding as a water Čerenkov muon veto detector. The detector components are carefully modeled in the simulation. The liquid scintillator is Pseudocumene with the addition of a 1.5 g/l fraction of wavelength shifter 2,5-diphenyl-oxazole ($C_{15}H_{11}NO$). The FLUKA simulation also implemented the photo-sensors of the inner detector, but no attempt was made to include optical transport, or to address the creation of detector signals at this point because of computational time considerations. However, the production of cosmogenic isotopes as well as neutron capture reactions on hydrogen inside the Inner Vessel were recorded.

4.2 Benchmark results

4.2.1 Muon-induced neutron yield

The concept of neutron yield was given in [1] as “the number of neutrons produced by one fast muon per $g\ cm^{-2}$ ”, and predicted by theory to increase with the mean muon energy approximately as $\overline{E}_\mu^{0.7}$. However as defined, this quantity is not accessible to experiment. Underground experiments record the capture of thermalized neutrons in liquid scintillator detectors. In part, this is necessary because of the large initial energy deposited by the parent muon(s) so that only delayed neutron capture signals can be identified. Borexino reports the cosmogenic muon-induced thermal neutron capture yield in liquid scintillator, ignoring fast neutron capture reactions on carbon which are predicted to only account for approximately 1% of neutron captures. Further, a fraction of the created energetic neutrons re-interact, and not all nuclear reactions will have neutrons in the final state. The predicted discrepancy between the total number of neutrons created during cosmogenic

events as opposed to the number of thermal neutron captures, is somewhat less than 10% for a liquid scintillator target. This discrepancy can only be addressed through modeling and is distinct from the frequently mentioned issue of “double counting neutrons”, which in simulation work only refers to (n,xn) type processes, with xn indicating ≥ 2 final state neutrons. Early published experimental results did not address this difference. In addition, the early experiments tried to assess the neutron production yield in standard rock rather than for liquid scintillator.

The reported experimental and FLUKA predicted neutron capture yields for Borexino [22] are:

	Yield [$\times 10^{-4}(\mu\text{on g/cm}^2)^{-1}$]
Borexino	3.10 ± 0.11
FLUKA prediction	2.46 ± 0.12

Table 3. Cosmogenic muon-induced neutron capture yield. Only statistical errors are given for the simulation.

The measured and the simulated neutron capture yields are shown by the solid and open red symbols, respectively, as a function of mean muon energy on the left in Figure 5. They are compared to the available experimental data on neutron production in liquid scintillator. The data are the originally published values of neutron yield and mean muon energy ¹. The solid black symbols correspond to the historical measurements at increasing mean muon energy in GeV of 16.5 [7], 16.7 and 86 [2], 125 [3], 270 [4] and 385 [6]. More recent values are presented by the solid blue and green symbols from the KamLAND [28] and LVD [29] experiments, at mean muon energy of 260 and 280 GeV respectively.

The original theoretical prediction for the neutron yield in standard rock at depth is shown by the thick black line ². The prediction predates experimental information. It was stated that: “such calculations give the dependence on \overline{E}_μ to good accuracy, but absolute values are accurate only in the order of magnitude” [1]. Later fits of the predicted power law to the early data resulted in parameterizations of the neutron yield, as for example, reported in [30] and depicted by the thin gray curve. The blue curve shown is a parameterization which was derived from an early FLUKA simulation [27].

Finally, the red curve is added which compares the predicted neutron yield as suggested by [31]. This work is frequently quoted in context of simulations for cosmogenic muon-induced neutrons deep underground where the FLUKA predictions were modified by arbitrarily post-scaling the muon-induced neutron production, as a function of mean muon energy, in order to match the historical data. More recent data have revised the experimental yield downward comparable to the unmodified FLUKA prediction.

Extra care is required to interpret the early experimental data. The assigned experimental uncertainties seem optimistic when taking into account the less refined level of experimental information available at the time, and the lack of detailed Monte Carlo simulations. This is important since the early detectors were smaller and not well shielded and/or constructed with large amounts of mixed passive target materials in addition to liquid scintillator. Similar complications apply to the assigned mean muon energies. A reduced neutron yield is supported by the original theoretical prediction together with new quality measurements at mean muon energies of

¹The result reported by the Palo Verde experiment [7] did not provide a mean muon energy and the value reported in [27] is adopted here.

² Specifically, the calculations were carried out for an aluminum target. However, predictions for standard rock should be reduced on the order 10%.

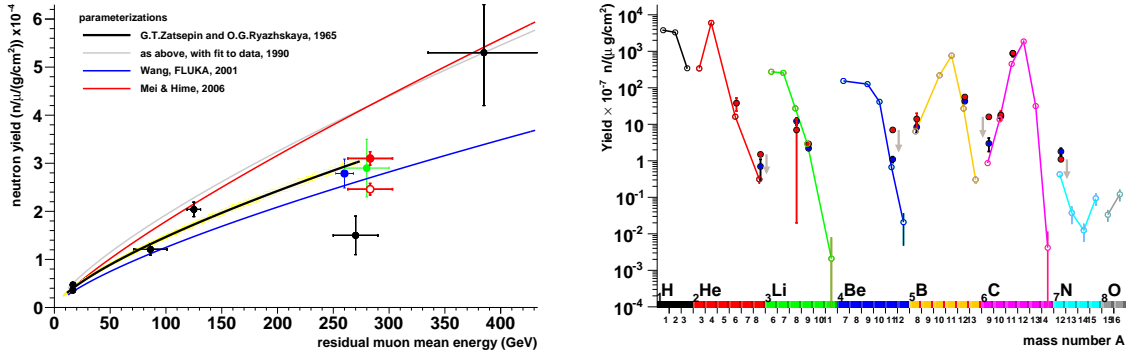


Figure 5. (left) Neutron capture yield as a function of mean muon energy with various representations of the experimental data. (right) Muon-induced cosmogenic isotope production yields in liquid scintillator at LNGS energies. Experimental results from Borexino (solid red symbols) and KamLAND (solid blue symbols) for some unstable isotopes are compared to FLUKA predictions. The Gray arrows indicated reported upper limits.

approximately 260 GeV and 283 GeV [22]. Note that FLUKA predictions and experimental data for the muon-induced neutron yield in liquid scintillator are now in fair agreement. These results are specific to light target materials and do not apply to heavy targets made of iron or lead.

4.2.2 ^{11}C isotope production

The creation of ^{11}C by cosmogenic muons in liquid scintillator was studied extensively by Borexino [22, 32] and the most recent experimental result is reported in Table 4. Approximately 30% of the cosmogenic neutrons measured in Borexino arise as final state neutrons in interactions leading to the creation of ^{11}C nuclides. Also listed in Table 4 is the FLUKA predicted ^{11}C yield. Only

	Yield [$\times 10^{-4}(\text{muon } g/\text{cm}^2)^{-1}$]
Borexino	0.886 ± 0.115
FLUKA prediction	0.467 ± 0.023

Table 4. Cosmogenic muon-induced production yield of ^{11}C . Only statistical errors are given for the simulation.

half as many ^{11}C nuclei are predicted as compared to the Borexino measurement. One reason for the low ^{11}C production rate in FLUKA is addressed by improvements to the Fermi break-up model [33] and these will be available with the next FLUKA release. In FLUKA, nuclear de-excitation is performed according to a Fermi break-up model for light nuclei with mass number $A \leq 16$. The updated model implements additional conservation laws as well as constraints on available final state configurations and symmetries. In the case of ^{11}C , the $\gamma + ^{12}\text{C}$ reaction in the current FLUKA model strongly favors break-up of ^{12}C into 3α over neutron emission via photo-production. However, the parity and spin of the 3α breakup is:

$$\gamma(1^-) + ^{12}\text{C}(0^+) \rightarrow 3\alpha(0^+).$$

Thus, the breakup into 3α particles with $L=0$ is forbidden even though this breakup is energetically favored. As a result, the reaction $^{12}\text{C}(\gamma, n)^{11}\text{C}$ is under-predicted by the current and previous FLUKA versions. An increase in the photoproduction of ^{11}C by a factor of 2 to 3 is expected with

the new model, see Figure 4 in [33]. The production of ^{11}C was studied with a beta version of FLUKA and the more than twofold increase of the ^{11}C new photoproduction rate was confirmed. Different reactions triggered by cosmogenic muon-induced secondaries also produce ^{11}C nuclei in liquid scintillator. The fraction of inclusive photoproduction contributes with 64% and the improved prediction for the ^{11}C production yield is $(0.70 \pm 0.02) \times 10^{-4} [(\mu\text{on g/cm}^2)^{-1}]$. Still this result is about 30% low with respect to experiment. The predicted fraction of ^{11}C production without a final state neutron is close to 10%.

Taking the improved ^{11}C production model into account, one could expect the predicted neutron capture yield to increase to approximately $2.7 \times 10^{-4} [(\mu\text{on g/cm}^2)^{-1}]$, which is within 15% of the reported experimental value. The FLUKA predictions for ^{11}C production in liquid scintillator can be compared to previous estimates [34] giving the rate of inclusive photoproduction at 60% and the fraction of ^{11}C production without final state neutrons at 5%. The missing, underpredicted neutrons due to the low ^{11}C yield, are expected to have a “softer” spectrum and are more easily removed by shielding.

4.2.3 Cosmogenic isotope production

The production yield for a list of unstable isotopes resulting from cosmogenic muon interactions in Borexino together with FLUKA predictions were reported in [22]. A similar study at comparable depth is available from the KamLAND experiment [28]. In Figure 5 on the right the experimental results are shown by the solid red and blue symbols for Borexino and KamLAND, respectively. They are compared to FLUKA predictions for the cosmogenic isotope production in liquid scintillator. Only an upper limit is reported by Borexino for some yields, and these are indicated in the graph by gray arrows. Good agreement between data and simulation is found considering the large variation in production yield spanning many orders of magnitude and the complexity involved in the simulation. As discussed in the previous section, the agreement for the ^{11}C production will improve with the next version of the FLUKA code, and predictions for other light isotopes may also be affected by these changes.

A recent FLUKA study for the Kamiokande water Čerenkov detector also reports good agreement for cosmogenic isotope production in a water target [35]. Liquid scintillator and water are two of the shielding media used for typical underground experiments and will be employed in this work.

4.2.4 Distance between neutron capture location and muon track

No information about the prompt neutron yield can be directly obtained from scintillation detectors due to the large initial signal caused by a penetrating muon(s) through the detector. However, the spatial reconstruction of the muon track and the delayed neutron capture locations in Borexino facilitate a study of the transverse distance neutrons can travel perpendicular to the parent muon track. In Borexino, only a single muon track is reconstructed per cosmogenic event since muon-bundles are not identified.

The lateral distribution of neutron captures from the parent muon track is shown in Figure 6. All the curves are normalized to permit comparison with the Borexino results. Both, the measured (red symbols) and the FLUKA predicted (solid black line) distributions from [22] are reproduced in the graph on the left. The muon track and the capture locations were constrained to lie within a radius, $R < 400$ cm, with respect to the detector center in order to obtain a clean data sample. Reconstruction uncertainties were applied *a posteriori* to the FLUKA predictions and these dominate the distribution at small distances from the parent muon track. The original

distributions are further compared to results from the LVD experiment [36] indicated by the solid green symbols. The shape of the experimental distributions is reproduced by the simulation.

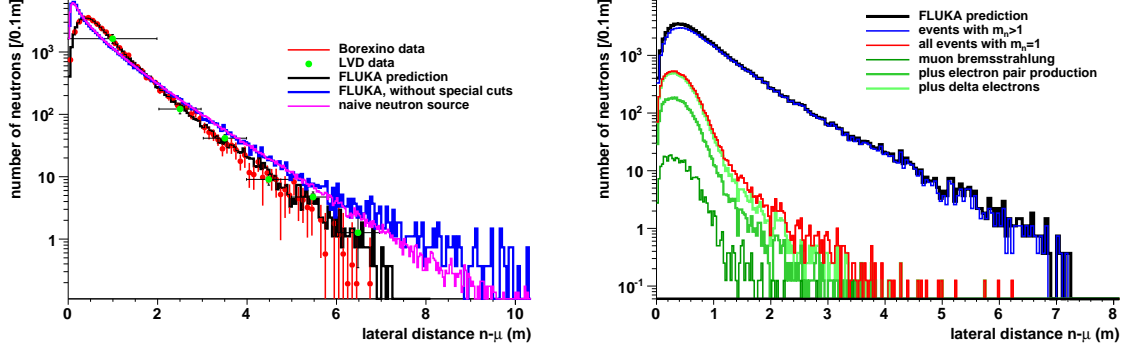


Figure 6. (left) Borexino experimental result, red symbols, and FLUKA predictions, black histogram, as reported in [22] are compared to a measurement from LVD [36], solid green symbols. The blue histogram gives the predicted lateral distribution before applying reconstruction uncertainties and additional radial cuts. This histogram is compared to the lateral distribution found from FLUKA for a simple neutron simulation (purple line), see text. (right) The predicted lateral neutron capture distribution, black histogram, is composed of neutrons from muon events producing many or single neutrons shown by the blue and red histograms respectively. For the latter, the cumulative fractions of events initiated by muon bremsstrahlung (dark green) electron pair production (green) and delta ray production (light green) are indicated.

The predicted lateral distance distribution without reconstruction uncertainties and no radial cuts is shown by the blue histogram in the same graph. Here, events with single muons crossing the Borexino Inner Detector were selected. The general shape of the distribution can readily be reproduced by assuming an isotropic neutron production around the muon track with an effective neutron diffusion length of approximately 90 cm. Note that only transverse information is accessible to experiment. This diffusion length is a very weak function of the kinetic energy for neutron energies above 200 MeV. Indeed one finds the purple histogram shown in Figure 6, when simulating a neutron beam with a flat kinetic energy spectrum ($E_{kin} < 350$ MeV) into liquid scintillator, and recording the lateral distance of thermal neutron capture locations with respect to the original neutron direction. Only at large distances does one see a small deviation from the predicted muon-induced neutron capture distance spectrum. However, this difference can be attributed to muon bundle events in the data since all neutrons are assigned to a single muon crossing the Borexino Inner Detector, and these could have been produced by coincident muons from bundles crossing the outer detector.

The predicted lateral distribution for Borexino is repeated on the right in Figure 6 by the solid black histogram. The contributions to this spectrum from events with a single neutron capture are shown by the red histogram as opposed to neutrons from events with higher neutron capture multiplicities given by the blue histogram. Muon-induced neutrons created in events with neutron multiplicity one, are predicted to capture substantially closer to the parent muon track.

The initial, discrete muon energy loss process, which eventually leads to the neutron production, was identified for these events. The cumulative contribution from muon bremsstrahlung (dark green), electron pair production (green) and delta ray production (light green) are indicated. Muon-nuclear interactions with only one neutron created in the event together with a $< 1\%$ contamination from negative muon capture, account for the small remaining difference to the red histogram.

4.2.5 Neutron multiplicity

In Figure 7 the multiplicity of thermal neutron captures per muon-induced cosmogenic event is shown. Both the Borexino experimental result (red symbols) and the FLUKA predicted distributions (black histogram) from [22] are reproduced in the graph on the left. This comparison is absolute which is different from that of the lateral distance distribution. The measured distribution is biased at large multiplicities due to detector performance with respect to energetic and/or muon bundle events. This effect was best reproduced in the simulation by selecting only events with single muon tracks crossing the Borexino inner volume. Good agreement in the shape of the distribution is found except at very low neutron multiplicity events.

“Hard” energy losses by energetic muons, which in turn can produce nuclear showers, are more likely initiated by muon bremsstrahlung and muon-nuclear interactions. The contribution to the neutron multiplicity spectrum attributed to both muon bremsstrahlung and muon-nuclear interactions is shown by the dashed green line. “Soft” energy losses on the other hand proceed mainly via electron pair and delta electron production (ionization). Their contribution to the neutron multiplicity spectrum is shown by the dashed blue line. The fraction of the individual muon interaction types which result in the capture of cosmogenic neutrons as a function of neutron capture multiplicity are given in the graph on the right in Figure 7. Almost 90% of the events which feature a single neutron capture are triggered by muons after delta electron and electron pair production.

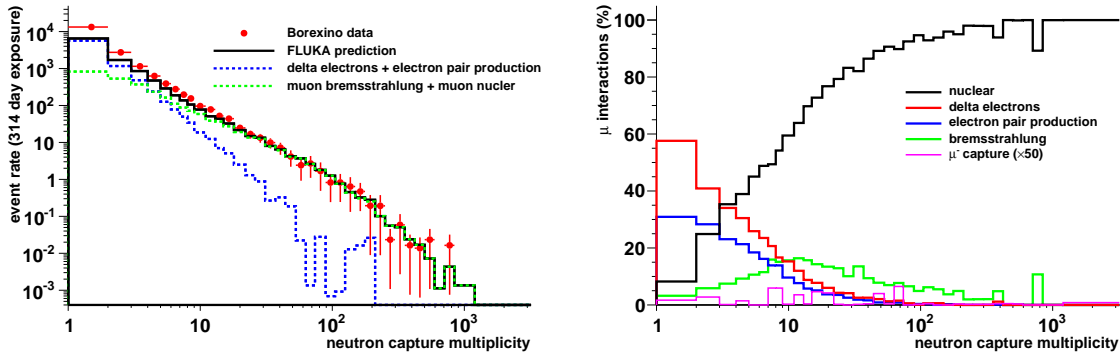


Figure 7. (left) Absolute comparison of muon-induced cosmogenic thermal neutron capture multiplicity as measured by Borexino, red symbols, and predicted by FLUKA, black histogram. For the simulated spectrum contributions from muon interactions associated with “soft” (dashed blue line) and “hard” (dashed green line) energy loss processes are shown separately. (right) Fractions of different muon interactions which trigger the production of neutrons in liquid scintillator as a function of neutron capture multiplicity. The fraction of μ^- capture is magnified by a factor of 50 for visibility.

The electromagnetic interaction of muons is well known and this has been carefully benchmarked in FLUKA. As reported in section 2.2, muon-nuclear interactions in FLUKA are simulated via virtual photon interactions. However, only incoherent interactions on single nucleons are simulated at low energy while coherent muon interactions, with multiple nucleons are expected to contribute. These “soft” muon-nuclear interactions are not implemented in the present FLUKA code, and may account for at least some of the underpredicted yield in Figure 7(left).

4.2.6 Muon rate producing neutrons

The reported rate of cosmogenic muon events resulting in one or more thermal neutron captures in Borexino is 67 ± 1 per day. The corresponding FLUKA simulated rate of 41 ± 3 per day is quite

low compared to experiment. The difference is limited to muon events with very low neutron capture multiplicities as is apparent from the spectrum shown on the left in Figure 7. According to FLUKA, these events are predominantly triggered by muon electron pair and delta electron creation, which generally yield neutrons with a “softer” energy spectrum. In addition, neutrons created in muon events with low neutron multiplicity, capture substantially closer to the parent track. This was shown in Figure 6 on the right for events with single neutron captures. This discrepancy, when compared to low energy, coherent muon-nuclear interactions, is still under investigation. Hence, even though the FLUKA predicted neutron event rate is approximately 30% low, the class of affected neutrons is less problematic in view of cosmogenic background suppression. Furthermore, because only those events with very low neutron multiplicities are affected, the impact on the neutron yield is less pronounced.

5 Cosmogenic background predictions for DarkSide

The DarkSide experiment is installed inside the Counting Test Facility (CTF) which is located in Hall C at LNGS adjacent to the Borexino detector. Because of the proximity of these two experiments, the same muon induced cosmogenic radiation field which was prepared for Borexino can also be used to simulate the cosmogenic background for DarkSide. This presents the unique opportunity to validate the simulation ansatz, to normalize the predictions to the *in-situ* measured muon flux, and to study systematic uncertainties of the simulation procedure for a ton-sized dark matter experiment.

5.1 Detector geometry

The DarkSide detector consists of a cylindrical, two-phase underground liquid argon Time Projection Chamber (TPC) [37]. The TPC is contained inside a thin-walled stainless steel Dewar. The sensitive region is viewed by photomultiplier tubes from the top and bottom. It is surrounded by a TPB³ coated Teflon cylinder which acts as an optical reflector and wavelength shifter. The Teflon cylinder also supports a set of copper rings which provide the electric field. The DarkSide-50 experiment with an active mass of 50 kg, is currently under commissioning. It features a sensitive volume of about 35 cm diameter and 35 cm height. The inner detector is immersed in a highly efficient, borated Liquid-Scintillator neutron Veto (LSV) to reduce external backgrounds and to monitor cosmogenic and radiogenic neutron backgrounds *in situ*. To further reduce cosmogenic backgrounds, the LSV is surrounded by ultra pure water inside a large cylindrical water tank (CTF) which functions as muon veto Čerenkov detector. The CTF also provides a passive shield against low energy external backgrounds. The implementation of DarkSide in FLUKA is shown in Figure 8.

In addition to its scientific reach, DarkSide also serves as a prototype for the development of a ton-sized, next generation TPC. The present design of the veto detector system permits the upgrade to DarkSide-G2 with a sensitive mass of approximately 3.3 tons using underground liquid argon depleted of the ³⁹Ar isotope. The ton-sized TPC features a sensitive volume of about 150 cm diameter and 135 cm height. In general, the rate of cosmogenic neutron background scales with the size of the sensitive detector volume and is substantially larger for DarkSide-G2 compared to that of DarkSide-50. Similarly, the increased size of the TPC displaces a larger amount of liquid scintillator inside the LSV and reduces the efficiency of detecting neutrons.

³Tetraphenyl butadiene, fluorescent die

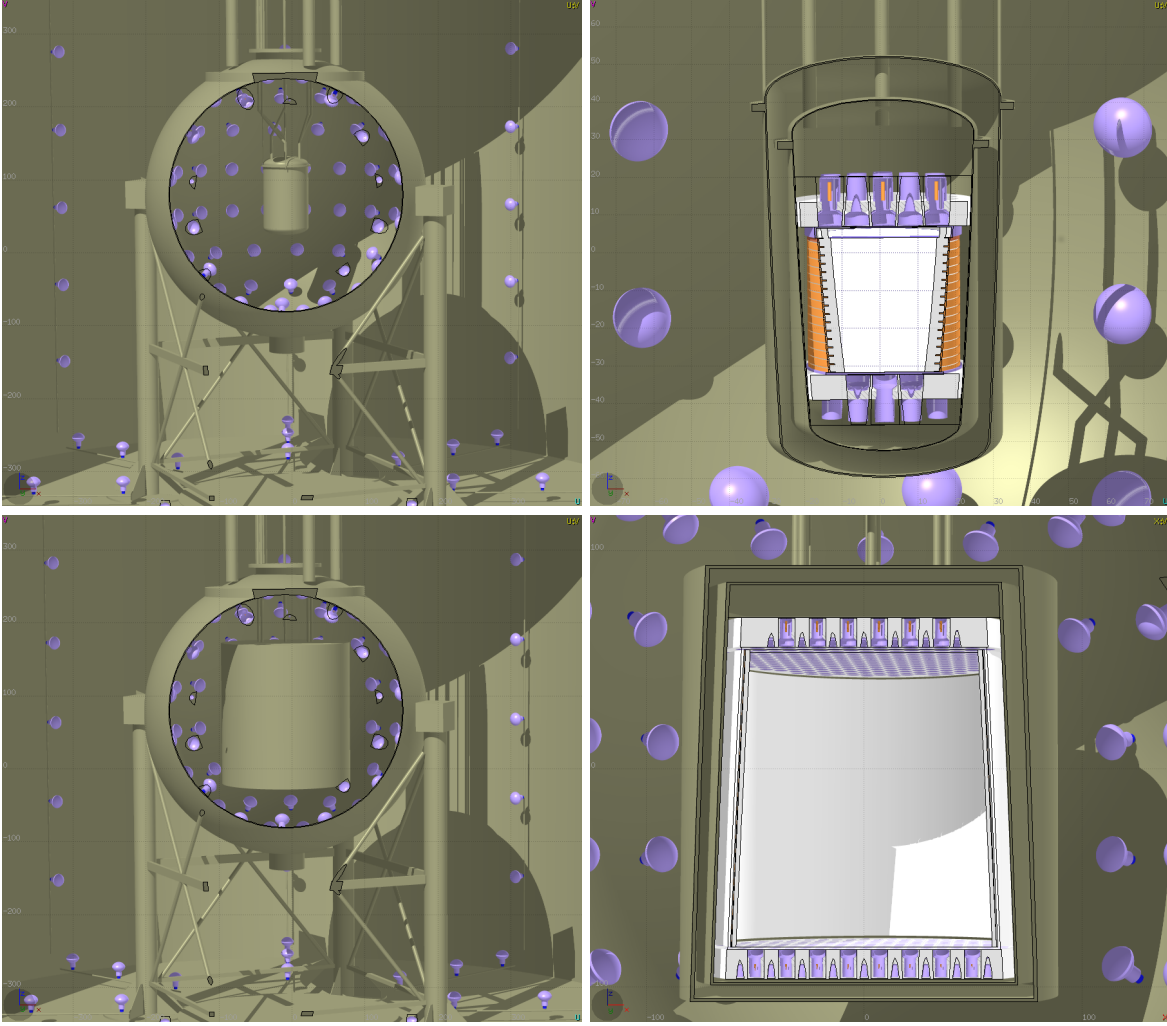


Figure 8. FLUKA implementation of the DarkSide experiment. The Dewar containing the TPC is shown mounted inside the LSV on the left while the graphs on the right expose details of the geometry implemented for the TPC. Top row: DarkSide-50; Bottom row: DarkSide-G2.

5.1.1 Counting Test Facility

The CTF [38] is modeled in this simulation as a cylindrical tank of 11 meter diameter and 10 meter height constructed from 8 mm thick carbon steel. It is filled with ultra pure water and placed on an additional 10 cm thick layer of steel. The inside tank surfaces are covered by sheets of a special type of layered Tyvek foil [39] to enhance light collection. For the relevant spectral range determined by the produced Čerenkov light and the sensitivity of the PMTs, a reflectivity in water of greater than 95% is expected. However, in the simulation a more conservative constant reflectivity of 80% was assumed. Čerenkov light produced in the water is measured by 80 ETL-9351 eight-inch PMTs which are placed along the floor and the walls of the CTF. The production, propagation and detection of the Čerenkov photons in the CTF is simulated in detail by FLUKA using a constant refractive index of 1.334 and a realistic absorption spectrum for pure water [40]. The photo sensors are modeled with their measured quantum efficiency spectrum scaled by a 70% photoelectron collection efficiency [41]. A study to evaluate the placement of the PMTs indicated

only a weak dependence of the overall efficiency as a function of the spatial distribution of the optical sensors. The insensitivity to the spatial dependence is attributed to the low absorption in pure water combined with the high surface reflectivity.

5.1.2 Liquid-Scintillator neutron Veto

The LSV [42] is implemented as a 4 meter diameter stainless steel sphere with 8 mm wall thickness. It is filled with a borated liquid scintillator consisting of a 1:1 mixture of Pseudocumene and Trimethylborate. The sphere is located inside the CTF and both the inside and the outside surfaces are covered by the Tyvek reflector. The LSV is equipped with 110 low-background glass-bulb Hamamatsu R5912-HQE-LRI eight-inch PMTs which are mounted on the sphere facing inward. Optical processes inside the LSV were not simulated. Instead, the un-quenched raw energy deposition per event is recorded.

5.1.3 Inner detector

Both, the DarkSide-50 and the DarkSide-G2 [37] configurations of the inner detector were implemented in the FLUKA simulation. Initial studies were carried out for the smaller DarkSide-50 design, however the following results are for the ton-sized DarkSide-G2 geometry. In this case, the cosmogenic background requirements are more stringent as DarkSide-G2 has a much larger sensitive volume. Thus the results can be viewed as a conservative upper limit to those expected for DarkSide-50. The geometry and material composition of the Dewar and TPC for the DarkSide-50 setup were modeled in detail according to the latest detector design drawings. This was then used to prepare a realistic, scaled model for the ton-sized configuration. In the simulation the sensitive volume is viewed by 283 three-inch Hamamatsu, low-background R11065 PMTs positioned on the top and an equal number on the bottom of the TPC. As for the LSV, no simulation of the optical processes inside the TPC were undertaken. The number of particles entering the sensitive volume, their type and the total raw energy deposited per event were recorded.

5.2 Simulation results

As described above, events which were “frozen” on the walls inside of the experimental Hall C at LNGS, were transported by FLUKA through the section of the cavern which contains the DarkSide-G2 experiment. Results are presented based on a total number of simulated cosmogenic events corresponding to a lifetime of approximately 34 years. The statistical uncertainty of the results is on the order of a few percent, and in any event, is smaller than the systematic uncertainties. Events for which at least one particle reached the CTF water tank were recorded as a first step. The predicted rate for these cosmogenic events at the outside of the CTF is approximately 3.45 events per minute. For about 23% of the events, the original cosmogenic muon does not reach the CTF water tank.

In a second step of the simulation, the complete DarkSide-G2 detector setup was then exposed to all events which were recorded at the outside of the CTF. All physics processes were turned on making use of the FLUKA defaults setting PRECISIO(n). In this step of the simulation Čerenkov photons were created inside the CTF water tank. However, because of CPU considerations they were not initially transported. The rate of cosmogenic events with at least one particle reaching the LSV is predicted to be approximately 0.30 events per minute. This reduction in rate is the result of both the smaller size of the volume and the passive shielding of the water tank. Similarly, the rate of cosmogenic events with at least one particle reaching the sensitive region inside the TPC is predicted by FLUKA to be 0.07 events per minute. Reported

rates are upper limits since no energy deposition in the respective detectors was required. The expected cosmogenic event rates are summarized in Table 5.

Table 5. Expected cosmogenic event rates	
just outside of	cosmogenic event rate (per minute)
CTF	3.45
LSV	0.30
sensitive liquid argon region	0.07

In order to further study the predicted cosmogenic background for the DarkSide-G2 experiment, the subset of events with at least one particle reaching the inner sensitive region was considered. In Figure 9 the raw energy deposited inside the CTF and the LSV are graphed with respect to each other. Cosmogenic events with at least one particle reaching the sensitive liquid argon volume almost always deposits a significant amount of energy inside the veto detectors. The dominant region in the scatter plot is indicated by the red box and limited by $dE_{(CTF)} > 1.3$ GeV and $dE_{(LSV)} > 0.2$ GeV.

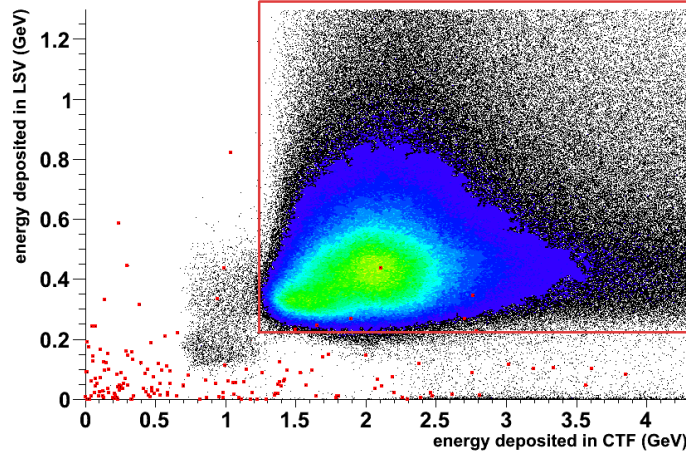


Figure 9. Energy deposition inside CTF and LSV for cosmogenic events with at least one particle reaching the sensitive volume of the inner detector.

This region corresponds to events with the original cosmogenic muon traversing both outer detectors. The superimposed color contour plot indicates the shape of the most frequent energy deposition for cosmogenic events resulting from the ionization of the relativistic muons. Events with similar energy deposited inside the CTF but with $dE_{(LSV)} < 0.2$ GeV indicate that the original muon traversed the CTF but missed the LSV. A smaller set of events in the region of $0.7 \text{ GeV} < dE_{(CTF)} < 1.3 \text{ GeV}$ results from low energy cosmogenic muons which traverse the water tank but stop inside the LSV.

The most difficult cosmogenic events to veto are found close to the origin of the graph. For these events, little energy is deposited both inside the CTF and the LSV. Cosmogenic events predicted by FLUKA without a direct muon into the CTF are superimposed on the graph with solid red symbols. Approximately 7.9 of these events per year are expected according to the simulation. Practically all cosmogenic events which have small energy deposition in both the CTF and LSV fall into the class of events with no direct muon entering the CTF.

The most important background events for the direct dark matter search consist of neutron-induced recoils in the sensitive volume from undetected neutrons. In the next step of the simulation, all events for which at least one neutron (but < 50 coincident particles⁴) reached the sensitive liquid argon region were reprocessed with full treatment of optical processes inside the CTF. A total of 19735 of these events, or 581 events per year, are predicted by FLUKA. Only the raw energy deposited inside the LSV and the sensitive region of the TPC are available in the current simulation. Therefore, conservative criteria were defined to select events which are considered detectable by the LSV: $dE_{(LSV)} > 1$ MeV, and for events which fall into the energy range of a possible dark matter signal in the TPC: $0 < dE_{(TPC)} < 1$ MeV [43].

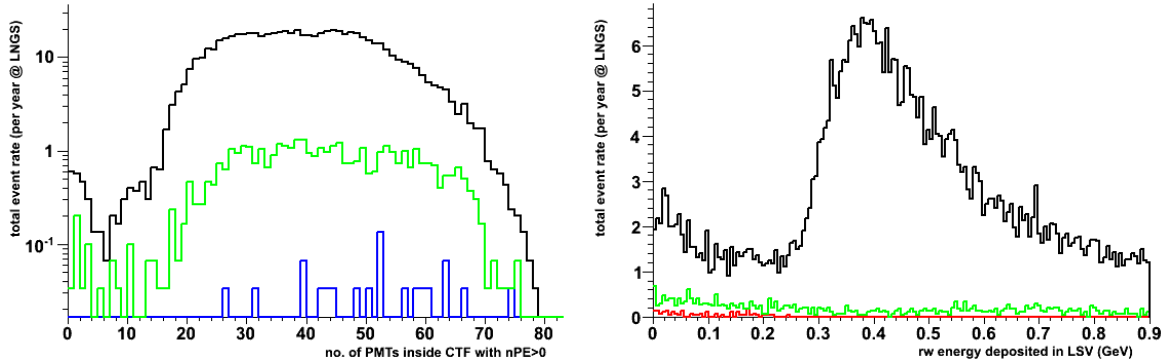


Figure 10. (a) Number of PMTs with at least 1 registered photoelectron. black: all events, green: raw dE inside TPC > 0 and < 1 MeV, and blue: raw dE inside the LSV < 1 MeV. (b) Un-quenched energy deposited inside the LSV. black: all events, green: raw dE inside TPC > 0 and < 1 MeV, and red: < 10 PMTs with at least 1 registered photoelectron.

The predicted response of the veto detectors is shown in Figure 10 for an equivalent lifetime of approximately 34 years. The number of events found for the CTF as a function of PMTs which register a signal (one or more photoelectrons) is given by the black histogram on the left. The events shown by the blue histogram are found if the energy deposited inside the LSV is limited to less than 1 MeV. The black histogram in the graph on the right shows the predicted energy spectrum for the LSV. Limiting the sample to events with less than 10 PMTs which register a signal inside the CTF reduces the energy spectrum to the events shown by the red histogram. The effect of selecting events in the energy range of interest for the TPC is indicated for both distributions by the green histograms.

The same information with focus on events with energy less than 14 MeV deposited in the LSV are shown in Figure 11. The number of PMTs with a signal inside the CTF is graphed versus the raw energy deposited in the LSV. Ten events with less than 3 PMTs recording a signal inside the CTF are considered to be missed by the muon veto and are colored red in the plot. Similarly, twenty-one events with a raw energy deposition of less than 1 MeV inside the LSV are considered missed and are colored blue in the graph.

The FLUKA simulation predicts approximately 581 events per year in which at least one cosmogenic muon-induced neutron enters the sensitive liquid argon volume. Out of these events, only 0.3 events per year fail to cause a signal in 3 or more PMTs of the CTF muon Čerenkov veto. At the same time, only 0.6 events per year deposit less than 1 MeV inside the LSV. For

⁴ This technical cut to reduce processing times only affects approximately 4% of the selected events. The suppressed events all deposit more than 2 GeV of raw energy in the LSV as well as the CTF.

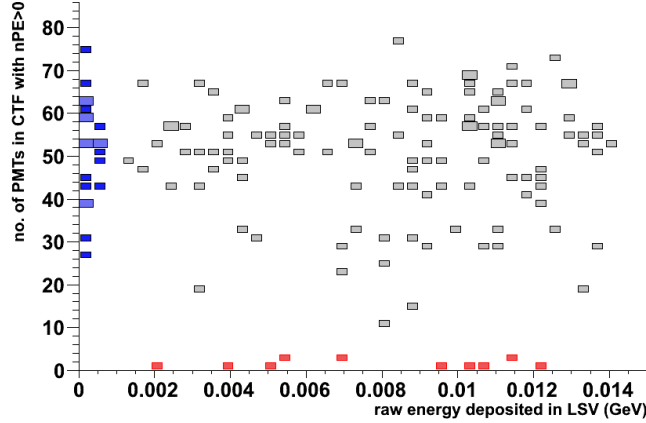


Figure 11. Shown is the of number of PMTs which registered at least one photoelectron inside the CTF versus the un-quenched energy deposited in the LSV. The red and blue color coded entries correspond to the respective events selected in Figure 8.

a simulated live-time of approximately 34 years at LNGS, no event where a neutron reached the sensitive liquid argon region but failed to trigger at least one of the two veto detectors is observed. These reported rates do not take advantage of additional discrimination information from the TPC which can be used to further reject cosmogenic neutron background.

The cosmogenic muon-induced neutron background rate to the DarkSide-50 experiment is significantly smaller than for the much larger DarkSide-G2 configuration, while the same veto detectors are used for both implementations. The rejection of external cosmogenic neutrons by the LSV increases for DarkSide-50 since there is more liquid-scintillator volume. In addition, this also increases the amount of passive shielding.

The presented background evaluation was based on cosmogenic muon-induced secondaries which are prompt and thus can be vetoed by the outer detector systems. The contribution from delayed neutrons after β -decay of muon-induced precursor nuclei, which are similar to detector internal radiogenic neutrons, are small as discussed in [44].

6 Conclusions

FLUKA predictions for cosmogenic muon-induced neutron backgrounds are found to be in reasonable agreement with available data. A few additional problems were identified and will be addressed in future versions of the FLUKA code. Corrections relating to the (γ, n) reaction on ^{12}C for example, can be approximately included in the final results, as was discussed in the text. However, the discrepancy and suggested correction reported in Ref. [31] were found invalid. On the other hand, a compelling analysis of the underpredicted single neutron multiplicity yield pointed to a potential problem in the missing contribution of low energy, electro-produced neutrons in FLUKA.

The need of a detailed description of the full muon-induced radiation field for the considered underground site was described and shown to be important. Steps to explicitly prepare the cosmogenic radiation field with the FLUKA simulation package were described and the muon-induced radiation field which was used to carry out benchmark studies, was then applied to the DarkSide experiment. Background predictions for a direct dark matter search experiment were obtained for the next generation, ton-sized two-phase underground liquid argon detector. It was

found that the proposed dual active-veto system for the experiment provides sufficient shielding against cosmic radiation at the LNGS depth for a ton-sized DarkSide-G2 experiment for more than 5 years.

Background levels for the DarkSide-50 experiment, which makes use of the same veto detector system, are expected to be significantly reduced because of the smaller size and the consequently increased volume of the liquid-scintillator shield and thus adequate for the smaller detector. In the future it is essential to monitor the cosmogenic neutron background levels, with focus on the veto detector system, in order to continue to benchmark the simulation.

Acknowledgments

This work was supported in part by NSF awards 1004051 and 1242471. We would like to thank Alfredo Ferrari and Maximilliano Sioli for FLUKA related help and acknowledge the use of the FLUKA graphical user interface FLAIR. We also would like to thank Davide D'Angelo, Quirin Meindl and Michael Wurm of the Borexino collaboration. Finally, we like to thank Vitaly Kudryavtsev for lively discussions, in particular about early measurements of the muon-induced neutron yield.

References

- [1] O. G. Ryajskaya and G. T. Zatsepin, *Depth-intensity curve of nuclear events induced by nuons*, *Proc. Int. Conf. Cosmic Rays* (1965).
- [2] L. B. Bezrukov et al., *Investigation of depth-intensity curve of nuclear events induced by muons*, *Sov. J. Nucl. Phys.* 17, 51 (1973).
- [3] R. I. Enikeev et al., *Hadrons generated by cosmic-ray muon underground*, *Sov. J. Nucl. Phys.* 46, 883 (1987).
- [4] M. Aglietta et al., *Measurement of the Neutron Flux Produced by Cosmic-Ray Muons with LVD at Gran Sasso*, *Proc. of the 26th ICRC, Salt Lake City, Vol 2* (1999).
- [5] F. F. Khalchukov et al., *Hadrons and other secondaries generated by cosmic-ray muons underground*, *Il Nuovo Cimento, Vol 18C, N.5* (1995).
- [6] M. Aglietta et al., *Neutron flux generated by cosmic-ray muons at 5200 hg/cm² s.r. underground. depth-neutron intensity curve.*, *Il Nuovo Cimento, Vol 12C, N.4* (1989).
- [7] F. Boehm et al., *Neutron production by cosmic-ray muons at shallow depth*, *Phys.Rev. D* 62 (2000) [000601].
- [8] G. Battistoni, S. Muraro, P. Sala, F. Cerutti, A. Ferrari, S. Roesler, A. Fassò, and J. Ranft, *The FLUKA code: Description and benchmarking*, *AIP Conference Proceeding* 896 (2007) 31–49.
- [9] A. Fassò, A. Ferrari, J. Ranft, and P. Sala, *FLUKA: a multi-particle transport code*, .
- [10] FLUKA Collaboration, *FLUKA manual, ASCII or .pdf file available from FLUKA website and contained in FLUKA package*, November, 2011.
- [11] A. Empl, E. V. Hungerford, R. Jasim and P. Mosteiro, *Simulation of Cosmogenic Backgrounds, A FLUKA Study, Not Yet Decided, to be published* (2012) [1210.2708].
- [12] L. B. Bezrukov and E. V. Bugaev, *Nucleon shadowing effects in photonuclear interactions*, *Sov. J. Nucl. Phys.* (May, 1981).
- [13] A. Fassò and A. Ferrari and J. Ranft and P. R. Sala, *FLUKA: Status and Perspectives for Hadronic Applications, Proceedings of the MonteCarlo 2000 Conference, Lisbon* (2001) 159–164.

- [14] A. Fassò and A. Ferrari and J. Ranft and P. R. Sala, *FLUKA, Performances and Applications in the Intermediate Energy Range, Proceedings of the "Specialists' Meeting on Shielding Aspects of Accelerators, Targets & Irradiation Facilities, Arlington"* (1995).
- [15] A. Ferrari and P. R. Sala, *Intermediate and high energy models in FLUKA: improvements, benchmarks and applications*, *Proceedings of Workshop on Nuclear Reaction Data and Nuclear Reactors Physics, Design and Safety, Trieste* (1998).
- [16] G. Battistoni and others, *Recent Developments in the FLUKA nuclear reaction models, Proceedings of 11th International Conference on Nuclear Reaction Mechanism, Varenna* (2006).
- [17] M. Brugger, A. Ferrari, S. Roesler, and L. Ulrici, *Validation of the fluka monte carlo code for predicting induced radioactivity at high-energy accelerators, NIM in Physics Research* **A562** (2006) 814–818.
- [18] G. Bellini and others, the Borexino collaboration, *Cosmic-muon flux and annual modulation in Borexino at 3800 m water-equivalent depth, Journal of Cosmology and Astroparticle Physics* **05(2012)015** (may, 2012) [[1202.6403](#)].
- [19] M. Ambrosio, the MACRO Collaboration, *High statistics measurement of the underground muon pair separation at gran sasso, Phys. Rev. D* **60** (Jun, 1999) 032001.
- [20] M. Ambrosio, the MACRO Collaboration, *Measurement of the residual energy of muons in the gran sasso underground laboratories, Astroparticle Physics* **19** (2003) 313–328, [[0207043v2](#)].
- [21] S. Ahlen, the MACRO Collaboration, *Muon Astronomy with the MACRO Detector, The Astrophysical Journal* **412** (1993) 301–311.
- [22] G. Bellini and others, the Borexino collaboration, *Cosmogenic Backgrounds in Borexino at 3800 m water-equivalent depth, JCAP* **08 (2013) 049** (2013) [[1304.7381](#)].
- [23] G. Battistoni, A. Margiotta, S. Muraro, and M. Sioli, *FLUKA as a new high energy cosmic ray generator, Nuclear Instruments and Methods in Physics Research Section A: Accelerators, Spectrometers, Detectors and Associated Equipment* **626-627** (2011) S191–S192.
- [24] J. T. Hong, the MACRO Collaboration, *Multiple muon measurements with macro, hep-ex/9410001* (1995) [[9410001v3](#)].
- [25] M. Ambrosio and others, the MACRO collaboration, *Vertical muon intensity measured with macro at the gran sasso laboratory, Phys. Rev. D* **52** (Oct, 1995) 3793–3802.
- [26] N. Agafonova and others, the OPERA collaboration, *Measurement of the atmospheric muon charge ratio with the OPERA detector, Eur. Phys. J. C* (2010) **67** (2010) 25–37.
- [27] Y. F. Wang, V. Balic, G. Gratta, A. Fassò, S. Roesler, and A. Ferrari, *Predicting neutron production from cosmic-ray muons, Phys. Rev. D* **64** (2001).
- [28] S. Abe et al., *Production of radioactive isotopes through cosmic muon spallation in KamLAND, Phys. Rev. C* **81** (February, 2010) [[0907.0066](#)].
- [29] R. Persiani and M. Garbini and G. Sartorelli and M. Selvi and LVD collaboration, *Measurement of the muon-induced neutron yield in liquid scintillator and stainless steel at LNGS with the LVD experiment, AIP Conf. Proc.* **1549, 235** (2013) (April, 2013).
- [30] L. V. Dadykin et al., *Study of Neutron Flux Generated by Cosmic Ray Muons at the Depth of 5200 hg/cm². Depth - Neutron Intensity Curve, Proc. of the 21th ICRC, Adelaide, V r90* (1999).
- [31] D.-M. Mei and A. Hime, *Muon-induced background study for underground laboratories, Phys. Rev. D* **73** (Mar, 2006) 053004.
- [32] G. Bellini et al., *Precision Measurement of the 7 Be Solar Rate in Borexino, Phys. Rev. Lett.* **107** (2011).

- [33] T. T. Bolen and others, *The FLUKA code: developments and challenges for high energy and medical applications*, *Proc. of International Conf. on Nuclear Data for Science and Technology*, New York, in press (2013).
- [34] C. Galbiati et al., *Cosmogenic ^{11}C production and sensitivity of organic scintillator detectors to pep and CNO neutrinos*, *Phys. Rev. C* **71** (2005).
- [35] S. W. Li and J. F. Beacom, *First calculation of cosmic-ray muon spallation backgrounds for MeV astrophysical neutrino signals in Super-Kamiokande*, to be published (March, 2014) [[1404.4687](#)].
- [36] V. A. Kudryavtsev, L. Pandola, and V. Tomasello, *Neutron- and muon-induced backgrounds in underground physics experiments*, *Eur.Phys.J* **A36** (2008) 171–180, [[0802.3566](#)].
- [37] P. D. Meyers, C. Galbiati, F. P. Calaprice, *DarkSide-50: A Direct Search for Dark Matter with New Techniques for Reducing Background*, *Proposal*, submitted by Princeton to DOE (April, 2011).
- [38] G. Alimonti, and others, the Borexino collaboration, *A large-scale low-background liquid scintillation detector: the counting test facility at Gran Sasso*, *NIM A* **406** (1998) 411426.
- [39] L. Wang and others, *Study of Tyvek reflectivity in water*, *Chinese Physics C* **36(7)** (2012) 628–632.
- [40] M. R. Querry, D. M. Wieliczka, D. J. Segelstein, *Handbook of Optical Constants of Solids II*, .
- [41] K. B. McCarty, *The Borexino Nylon Film and the Third Counting Test Facility*. PhD thesis, Princeton University, 2006.
- [42] A. W., P. Mosteiro, B. Loer, and F. Calaprice, *A Highly Efficient Neutron Veto Using BoronLoaded Liquid Scintillator*, *AIP Conf. Proc.* **1338** (2010) 44–48, [[1010.3609](#)].
- [43] C.E. Aalseth and others, the DarkSide collaboration, *The DarkSide multi-ton detector for the direct dark matter search*, *Advances in High Energy Physics*, Article in Press (2014).
- [44] A. Empl and E. V. Hungerford, *A FLUKA Study of β -delayed Neutron Emission for the Ton-sized DarkSide Dark Matter Detector*, Not Yet Decided, to be published (2014) [[1407.6628](#)].